EARTHQUAKE ENGINEERING AND STRUCTURAL DYNAMICS
Earthquake Engng. Struct. Dyn. **27**, 673–685 (1998)

A HYBRID TIME FREQUENCY DOMAIN FORMULATION FOR NON-LINEAR SOIL–STRUCTURE INTERACTION

DIONISIO BERNAL*,† AND AKRAM YOUSSEF‡
Northeastern University, Boston, MA 02115, U.S.A.

SUMMARY

Methods that combine frequency and time domain techniques offer an attractive alternative for solving Soil–Structure-interaction problems where the structure exhibits non-linear behaviour. In the hybrid-frequency-time-domain procedure a reference linear system is solved in the frequency domain and the difference between the actual restoring forces and those in the linear model are treated as pseudo-forces. In the solution scheme explored in this paper, designated as the hybrid-time-frequency-domain (HTFD) procedure, the equations of motion are solved in the time domain with due consideration for non-linearities and with the unbounded medium represented by frequency-independent springs and dampers. The frequency dependency of the impedance coefficients is introduced by means of pseudo-forces evaluated in the frequency domain at the end of each iteration.

A criterion of stability for the HTFD approach is derived analytically and its validity is sustained numerically. As is often the case, the criterion takes the form of a limit of unity on the spectral radius of an appropriately defined matrix. Inspection of the terms in this matrix shows that convergence can be guaranteed by suitable selection of the reference impedance. The CPU times required to obtain converged solutions with the HTFD are found, in a number of numerical simulations, to be up to one order of magnitude less than those required by the alternative hybrid-frequency-time-domain approach. © 1998 John Wiley & Sons, Ltd.

KEY WORDS: soil–structure interaction; non-linear response; seismic analysis.

1. INTRODUCTION

In the analysis of soil–structure-interaction (SSI) problems using the substructure technique the unbounded soil is represented by its dynamic stiffness (impedance) for the degrees of freedom at the soil–structure interface. When the structure is linear the equations for the structure–soil system are most conveniently solved in the frequency domain, where the frequency dependency of the impedance coefficients can be readily considered.[1] It is well known, however, that buildings are typically designed in such a way that significant inelastic behaviour can be anticipated in the event of severe ground motion. To compute the dynamic response of a non-linear structure interacting with an unbounded soil, methods that work in the time domain become necessary.[2–4] The salient feature of a time domain approach is the evaluation of the interaction forces at the soil–structure interface. In particular, it can be shown that these forces depend on the history of the displacements at the boundary up to the time of interest and, as a consequence, need to be described in terms of convolution integrals. While computational strategies involving recursive algorithms can be used to

* Correspondence to: Dionisio Bernal, Department of Civil Engineering, Northeastern University, 427 Snell Engineering Center, Boston, MA 02115, U.S.A. E-mail: bernal@neu.edu
† Associate Professor, Civil and Environmental Engineering
‡ Graduate Student

Contract/grant sponsor: Spanish Ministry of Education and Research

CCC 0098–8847/98/070673–13$17·50

Received 10 June 1997
Revised 6 November 1997

evaluate these integrals efficiently,[5–7] the mathematical complexity of the rigorous time domain formulation detracts from its use in routine analysis of non-linear soil–structure-interaction problems.

A strategy that offers conceptual simplicity and permits consideration of inelastic behaviour in the structure is the hybrid-frequency-time-domain procedure.[8–13] In this method, the equations of motion for a certain reference linear system are solved in the frequency domain (where the frequency dependency of the impedance is considered in the usual fashion) and the non-linear effects are evaluated in the time domain and treated as pseudo-forces. An undesirable feature of the hybrid-frequency-time-domain approach, however, is the fact that the pseudo-forces depend on the degree of non-linearity in the structure and can become very large during iterations, causing divergence. In fact, as illustrated by Darbre and Wolf,[9] successful implementation of this procedure typically requires that the iterations be carried out considering only a reduced number of time steps at a time. Also taking away from the attractiveness of the hybrid-frequency-time-domain technique is the fact that the number of iterations to attain convergence, when significant inelastic behaviour is involved, is typically large.

An alternative hybrid solution scheme, designated as the hybrid-time-frequency-domain (HTFD) approach, is explored in this paper. In the HTFD procedure, the soil is represented using frequency-independent springs, dashpots, and possibly masses, and the equations of motion are solved in the time domain with non-linearities in the structure considered in the usual way. The difference between the interaction forces corresponding to the actual impedance of the soil and that of the reference system used in the integration of the equations is accounted for by means of pseudo-forces which are easily evaluated in the frequency domain at the end of each iteration. As one gathers from the foregoing outline, the pseudo-forces in the HTFD procedure are restricted to the degrees of freedom (DOF) at the soil–structure interface and are not explicit functions of the extent of inelasticity. These features, coupled with the fact that only linear operations are needed to evaluate the pseudo-forces, makes implementation of the HTFD procedure particularly simple. As will be shown, solutions of non-linear SSI problems with the HTFD procedure are generally much more efficient than those obtained using the hybrid-frequency-time-domain technique.

As with any other iterative approach, identification of the conditions that govern convergence of the HTFD procedure is of fundamental importance. After presenting the mathematical description of the method in Section 2, the paper focuses on the derivation and testing of a convergence criterion. As is often the case, the convergence criterion developed is expressed as a limit of unity on the spectral radius, ρ, of a properly defined matrix. It is found that this matrix is a function of (a) the difference between the reference impedance used in the time-domain integration and the singular impedance; (b) the value of the regular part of the dynamic stiffness of the soil at $t = 0$; and (c) the characteristics of the numerical integration algorithm used.

An examination of the expressions derived in the analysis of convergence suggests that inelastic behaviour in the structure has a small effect on the stability limit of the HTFD procedure. Numerical simulations confirm this observation and show that in typical applications convergence is attained without difficulty. The paper concludes with an exploratory investigation of the relative efficiency of the HTFD approach compared to the hybrid-frequency-time-domain procedure.

2. THE HTFD METHOD

Following the well-established notation used in the SSI literature, we designate the nodes associated with the structure as s and those at the interface between the structure and the soil medium as b (Figure 1). The dynamic stiffness matrix for the soil with the excavation considered and for the excavated domain are given by $[S^{g}_{bb}(i\omega)]$ and $[S^{e}_{bb}(i\omega)]$, respectively, and the sum of these two impedances is designated as $[S^{f}_{bb}(i\omega)]$. With the total displacement vector as $\{u\}$ the equation of motion can be written as

$$\begin{bmatrix} [M_{ss}] & [M_{sb}] \\ [M_{bs}] & [M_{bb}] \end{bmatrix} \begin{Bmatrix} \{\ddot{u}_s(t)\} \\ \{\ddot{u}_b(t)\} \end{Bmatrix} + \begin{bmatrix} [C_{ss}] & [C_{sb}] \\ [C_{bs}] & [C_{bb}] \end{bmatrix} \begin{Bmatrix} \{\dot{u}_s(t)\} \\ \{\dot{u}_b(t)\} \end{Bmatrix} + \begin{Bmatrix} \{P_s(t)\} \\ \{P_b(t)\} \end{Bmatrix} + \begin{Bmatrix} \{0\} \\ \{R_b(t)\} \end{Bmatrix} = \begin{Bmatrix} \{0\} \\ \{L(t)\} \end{Bmatrix} \tag{1}$$

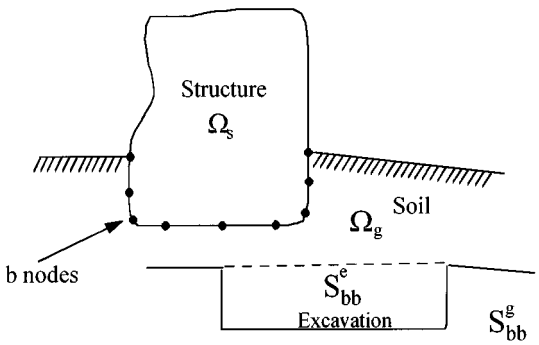

Figure 1. Structure–soil domains

where the driving loads $\{L(t)\}$ and the interaction forces $\{R_b(t)\}$ can be expressed as

$$\{L(t)\} = \frac{1}{2\pi}\int_{-\infty}^{\infty} [S^f_{bb}(\mathrm{i}\omega)]\{x_b(\mathrm{i}\omega)\}\mathrm{e}^{\mathrm{i}\omega t}\,\mathrm{d}\omega \tag{2}$$

and

$$\{R_b(t)\} = \frac{1}{2\pi}\int_{-\infty}^{\infty} [S^g_{bb}(\mathrm{i}\omega)]\{u_b(\mathrm{i}\omega)\}\mathrm{e}^{\mathrm{i}\omega t}\,\mathrm{d}\omega \tag{3}$$

In equation (1) $\{P(t)\}$ is the vector of restoring forces in the structure (which may be non-linear) and, in equation (2), $\{x_b(\mathrm{i}\omega)\}$ is the Fourier transform of the free field motion at the nodes located on the soil–structure interface. Equation (1) can be viewed as the second step in a solution based on superposition. The first part in this superposition is the response obtained when the degrees of freedom at the soil–structure interface are restrained while the second is the response to the negative of the restraining forces. Since the response at all DOF is zero in the first part, the solution of equation (1) yields the total displacements. It follows from the previous discussion that the vector $\{R_b(t)\}$ does not contain the actual interaction forces experienced during the response but rather a set of forces that enters into the calculation of the total displacements.

Passing $\{R_b(t)\}$ to the r.h.s. of equation (1) and adding the terms $[M_{\mathrm{ref}}]$, $[C_{\mathrm{ref}}]$ and $[K_{\mathrm{ref}}]$ to the partition associated with the b DOF one gets

$$\begin{bmatrix} [M_{ss}] & [M_{sb}] \\ [M_{bs}] & [M_{bb}] + [M_{\mathrm{ref}}] \end{bmatrix} \begin{Bmatrix} \ddot{u}_s(t) \\ \ddot{u}_b(t) \end{Bmatrix} + \begin{bmatrix} [C_{ss}] & [C_{sb}] \\ [C_{bs}] & [C_{bb}] + [C_{\mathrm{ref}}] \end{bmatrix} \begin{Bmatrix} \dot{u}_s(t) \\ \dot{u}_b(t) \end{Bmatrix} + \begin{Bmatrix} P_s(t) \\ P_b(t) + [K_{\mathrm{ref}}]\{u_b(t)\} \end{Bmatrix} = \begin{Bmatrix} 0 \\ L(t) \end{Bmatrix} - \begin{Bmatrix} 0 \\ \mathrm{PSF}(t) \end{Bmatrix} \tag{4}$$

where the pseudo-forces $\{\mathrm{PSF}(t)\}$ are given by

$$\{\mathrm{PSF}(t)\} = \{R_b(t)\} - [M_{\mathrm{ref}}]\{\ddot{u}_b(t)\} - [C_{\mathrm{ref}}]\{\dot{u}_b(t)\} - [K_{\mathrm{ref}}]\{u_b(t)\} \tag{5}$$

Introduction of $[M_{\mathrm{ref}}]$, $[C_{\mathrm{ref}}]$ and $[K_{\mathrm{ref}}]$ on the left-hand side of equation (4) implies that the reference impedance used to represent $[S^g_{bb}(\mathrm{i}\omega)]$ is $([K_{\mathrm{ref}}] - [M_{\mathrm{ref}}]\omega^2 + [C_{\mathrm{ref}}]\ \omega\mathrm{i})$. As noted in the introduction, equations (3) and (5) show that the pseudo-forces are restricted to the DOF at the soil–structure interface and that they do not depend explicitly on the degree of inelasticity in the structure.

In the HTFD procedure one solves equations (4) and (5) iteratively. Specifically, in a first iteration the pseudo-forces are taken as zero and equation (4) is integrated in the usual fashion. The time history of the

displacements at the soil–structure interface are then used to evaluate the pseudo-forces from equation (5). Using the computed pseudo-forces one solves equation (4) again and so on until some appropriately selected norm becomes equal to or smaller than a certain prescribed tolerance.

Since the response in a numerical solution is only available at a number of time stations ($n = 1, 2, \ldots, N$) a discrete version of equation (3) is utilized to compute $\{R_b\}$. Using the well-established notation for the fast Fourier transform operations one gets

$$\{R_b(n)\} = \mathrm{IFFT}([S^{\mathrm{g}}_{bb}(\mathrm{i}\omega)]\{u_b(\mathrm{i}\omega)\}) \tag{6}$$

where

$$\{u_b(\mathrm{i}\omega)\} = \mathrm{FFT}(u_b(n)) \tag{7}$$

2.1. Implementation issues

Implicit in the use of equations (6) and (7) is the fact that the interaction forces $\{R_b(t)\}$ are taken as the steady-state solution for a periodic expansion of $\{u_b(t)\}$. As is well known, good agreement between this periodic solution and the actual transient demands that spurious high frequencies be avoided in the transformation of $\{u_b(t)\}$ to $\{u_b(\mathrm{i}\omega)\}$. The importance of this requirement is made evident by the fact that the functions in$[S^{\mathrm{g}}_{bb}(i\omega)]$ do not decay with frequency and that, as a consequence, any spurious high-frequency components in $\{u_b(\mathrm{i}\omega)\}$ are amplified when obtaining $\{R_b\}$. In practice, this requirement is easily taken care of by appending a smooth decay function to the displacement vector $\{u_b\}$ prior to the Fourier transformation.[4] With the exception of very short segments which fail to attain the stated objective, it can be shown that the duration of the decay function has virtually no effect on the solution. A cubic polynomial which matches the displacement and the velocity at the end of the segment of desired results and spans 15 time steps is used in the numerical simulations presented in latter sections.

It is also appropriate, in bringing the periodic solution into coincidence with the transient, to follow the smooth transition with a quiet zone that allows the interaction forces to approach zero before the new period of imposed displacements starts. It is worth noting that because of the high inherent damping in the unbounded soil the length of the required quiet zone is typically very short. One can gain an appreciation for the required length of zero padding by considering the results depicted in Figure 2. The figure shows the overturning moment, computed using equations (6) and (7), for the shear building in Figure 3 subjected to the pulse in Figure 4. Three cases are plotted: (i) very long padding (transient), (ii) a quiet zone of 0·2 s (dimensionless time $t = tc_s/r_0 = 1$) and (iii) no padding. To accent the influence of periodicity the soil medium

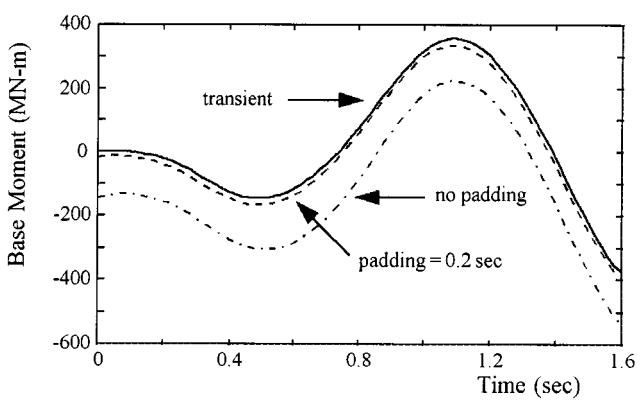

Figure 2. Time history of base moment for the building in Figure 3 (soil layer with $d/r_0 = 2$, excitation is the pulse in Figure 4, analysis duration = 1·6 s)

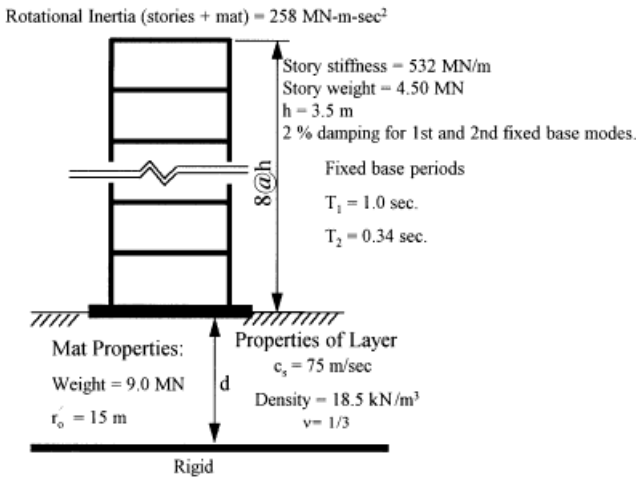

Figure 3. Shear building and foundation data

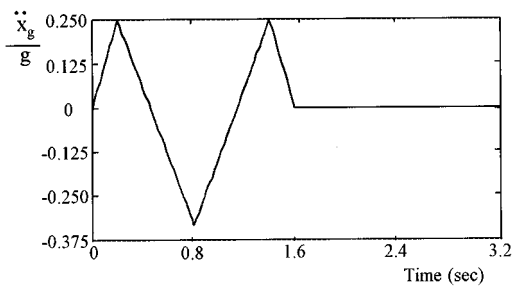

Figure 4. Ground acceleration pulse

is taken as an elastic layer with a depth twice the radius of the foundation, fixed at the base. For this condition, as Figure 5 shows, the impedance displays a cutoff frequency below which no radiation takes place.[14] One notes that although the effect of periodicity is clearly evident in the response for zero padding, the solution obtained with a padding of 0·2 s is already nearly identical to the transient.

3. CONVERGENCE CRITERION

Identification of the conditions for which stability is attained is of paramount importance in any iterative technique. The derivation of the stability limit presented in this section for the HTFD procedure is carried out in the time domain, where consideration can be given to the characteristics of the integration algorithm used to solve the equations of motion. Periodicity in the computation of the interaction forces is removed by using a causal expression relating $\{R_b(t)\}$ to $\{u_b(t)\}$. A discussion of the effect of periodicity when equations (6) and (7) are used to compute the interaction forces is presented in Section 4.

As noted previously, the pseudo-forces in equation (4) are associated exclusively with the DOF at the soil–structure interface. A consequence of this result is the fact that the convergence limit can be established by inspecting the partition associated with the b DOF, while the response at the s nodes are treated as known functions. The partition associated with the b DOF in equation (4) can be written in discrete form as

$$[\overline{M}_{bb}]\{\ddot{u}_b(n)\} + [\overline{C}_{bb}]\{\dot{u}_b(n)\} + [\overline{K}^t_{bb}]\{u_b(n)\} = \{Y(n)\} - \{\mathrm{PSF}(n)\} \tag{8}$$

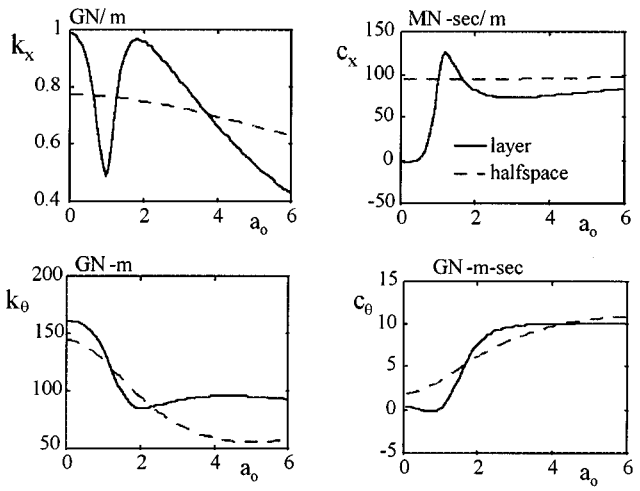

Figure 5. Impedance functions ($r_0 = 15$ m, $c_s = 75$ m/s, $v = 1/3$, layer with $r_0/d = 2$, $a_0 = \omega r_0/c_s$)

where the notation

$$[\overline{K}^t_{bb}] = [K^t_{bb}] + [K_{\text{ref}}] \tag{9}$$

$$[\overline{C}_{bb}] = [C_{bb}] + [C_{\text{ref}}] \tag{10}$$

$$[\overline{M}_{bb}] = [M_{bb}] + [M_{\text{ref}}] \tag{11}$$

has been introduced. In equations (8) and (9) the superscript t indicate reference to the tangent properties of the stiffness matrix. The vector $\{Y\}$ is used to collect the coupling terms as well as the values of the response at the b nodes prior to time $t = n\Delta t$. One can easily confirm that $\{Y(n)\}$ is given by

$$\{Y(n)\} = \{L(n)\} - [M_{bs}]\{\ddot{u}_s(n)\} - [C_{bs}]\{\dot{u}_s(n)\} - [K^t_{bs}]\{u_s(n) - u_s(n-1)\} - \{P_b(n-1)\} + [K^t_{bb}]\{u_b(n-1)\} \tag{12}$$

Assuming that the singular part of the impedance can be taken as a second order polynomial in $(i\omega)$ $\{R_b(t)\}$ can be written as

$$\{R_b(t)\} = [K_\infty]\{u_b(t)\} + [C_\infty]\{\dot{u}_b(t)\} + [M_\infty]\{\ddot{u}_b(t)\} + \int_0^t [S_r(\tau)]\{u_b(t-\tau)\}\,\mathrm{d}\tau \tag{13}$$

where the coefficients of the singular impedance are

$$[M_\infty] = -\frac{1}{2}\lim_{\omega\to\infty} \text{Real}\left(\frac{\mathrm{d}^2 S^{\text{g}}_{bb}(i\omega)}{\mathrm{d}\omega^2}\right) \tag{14}$$

$$[C_\infty] = \lim_{\omega\to\infty} \text{Im}\left(\frac{S^{\text{g}}_{bb}(i\omega)}{\omega}\right) \tag{15}$$

$$[K_\infty] = \lim_{\omega\to\infty} \text{Real}\,(S^{\text{g}}_{bb}(i\omega) + [M_\infty]\omega^2) \tag{16}$$

It is worth noting that while $[M_\infty]$ is typically zero when the foundation medium is assumed elastic, this matrix is non-zero for some components of motion when Poisson's ratio approaches 0.5.[2,15] The term $[M_\infty]$ has been included also to allow consideration of cases where Voigt damping is introduced (albeit approximately) by adding a term of the form $a\omega^2 + b\omega\mathrm{i}$ to the elastic impedance (where a and b are coefficients).[4]

The regular impedance, which vanishes as $\omega \to \infty$ is given by

$$[S_\mathrm{r}(\mathrm{i}\omega)] = [S^\mathrm{g}_{bb}(\mathrm{i}\omega)] - ([K_\infty] - [M_\infty]\omega^2 + [C_\infty]\mathrm{i}\omega) \tag{17}$$

As is well known, the regular part of dynamic stiffness in the time domain $[S_\mathrm{r}(t)]$, is given by the inverse Fourier transform of $[S_\mathrm{r}(\mathrm{i}\omega)]$;

$$[S_\mathrm{r}(t)] = \frac{1}{2\pi}\int_{-\infty}^{\infty} [S_\mathrm{r}(\mathrm{i}\omega)]\mathrm{e}^{\mathrm{i}\omega t}\,\mathrm{d}\omega \tag{18}$$

Substituting a discrete version of equation (13) into the equation for the pseudo-force (equation (5)) and the result into equation (8) one gets

$$[\overline{M}_{bb}]\{\ddot{u}_b(n)\} + [\overline{C}_{bb}]\{\dot{u}_b(n)\} + [\overline{K}^t_{bb}]\{u_b(n)\} = \{\overline{Y}(n)\} - \{Q(n)\} \tag{19a}$$

where

$$\{Q(n)\} = ([K_\infty] - [K_\mathrm{ref}] + [S^0_r]\Delta t)\{u_b(n)\} + ([C_\infty] - [C_\mathrm{ref}])\{\dot{u}_b(n)\} + ([M_\infty] - [M_\mathrm{ref}])\{\ddot{u}_b(n)\} \tag{19b}$$

In equation (19b), $[S^0_\mathrm{r}]$ is the magnitude of the regular part of the dynamic stiffness at $t = 0$ and,

$$\{\bar{Y}(n)\} = \{Y(n)\} - \Delta t \sum_{l=1}^{n} [S_\mathrm{r}(l)]\{u_b(n-l)\} \tag{20}$$

Note that since $\{\overline{Y}(n)\}$ does not depend on $\{u_b(n)\}$ it does not have an effect on the convergence limit of the iterative solution of equations (19a) and (19b).

3.1. *Iterative solution*

The convergence properties of the iterative solution of equations (19) are necessarily dependent on the algorithm used to perform the numerical integration. Consider the common case where the differential equations are converted into a set of algebraic equations of the form

$$[A]\{\Delta u\} = \{\Delta L\} \tag{21}$$

Equation (21) can be expressed in a form that applies in the case of an iterative solution by expressing $[A]$ as the sum of two matrices, namely,

$$[A] = [A_0] + [\Delta A] \tag{22}$$

Substituting equation (22) into equation (21) and noting that $\{\Delta u\} = \{u(n) - u(n-1)\}$ gives

$$[A_0]\{u(n)\} = \{\Delta L\} + [A]\{u(n-1)\} - \{R\} \tag{23a}$$

where

$$\{R\} = [\Delta A]\{u(n)\} \tag{23b}$$

By inspecting the series that results when equations (23a) and (23b) are solved iteratively one finds that after r iterations (to advance the solution from step $n-1$ to n) the vector $\{u(n)\}$ is given by

$$\{u(n)\}^r = \left[\sum_{m=1}^{r} (-1)^{m-1}([A_0]^{-1}[\Delta A])^{m-1}\right][A_0]^{-1}[\Delta L + [A]\{u(n-1)\}] \tag{24}$$

One concludes, from an inspection of the series in equation (24), that the condition that must be satisfied to ensure convergence is that the spectral radius of the matrix

$$[SR] = [A_0]^{-1}[\Delta A] \tag{25}$$

be less than unity. Where the spectral radius ρ is defined as the maximum of the absolute values of the eigenvalues in the matrix. When the Newmark-Beta method is used to transform equations (19) into the form of equation (21) one finds that the matrices $[A_0]$ and $[\Delta A]$ are given by

$$[A_0] = \frac{1}{\beta \Delta t^2}[\overline{M}_{bb}] + \frac{\gamma}{\beta \Delta t}[\overline{C}_{bb}] + [\overline{K}^t_{bb}] \tag{26a}$$

and

$$[\Delta A] = \frac{1}{\beta \Delta t^2}([M_\infty] - [M_{\text{ref}}]) + \frac{\gamma}{\beta \Delta t}([C_\infty] - [C_{\text{ref}}]) + [K_\infty] - [K_{\text{ref}}] + [S^0_{\text{r}}]\,\Delta t \tag{26b}$$

where γ and β are the parameters that control the stability and accuracy of the Newmark algorithm. As can be appreciated from equation (26a), the effect of inelasticity enters into the convergence limit through $[\overline{K}^t_{bb}]$.

3.2. *Calculation of* $[S^0_{\text{r}}]$

Equation (26b) shows that the magnitude of the regular part of the dynamic stiffness at $t = 0$ has an influence in the convergence limit of the HTFD procedure. In a numerical solution this matrix can be conveniently computed from equation (18). In particular, taking $t = 0$, recognizing that the functions in $[S_{\text{r}}(\text{i}\omega)]$ are odd and taking into consideration the fact that the functions in $[S_{\text{r}}(t)]$ are causal (and thus discontinuous at $t = 0$) one gets[16]

$$[S^0_{\text{r}}] = \frac{2}{\pi}\int_0^\infty [k_{\text{r}}(\omega)]\,\text{d}\omega \tag{27}$$

where $[k_{\text{r}}(\omega)]$ is the real part of $[S_{\text{r}}(\text{i}\omega)]$.

3.3. *Selection of the reference impedance*

A fundamental step in the implementation of the HTFD procedure is the selection of the reference impedance used to represent the unbounded soil in the time domain analysis. It is interesting to note that if the singular impedance is available, and is of the form assumed in equation (13), the spectral radius can be forced to zero by appropriate selection of the reference impedance. Specifically, from examination of equations (25) and (26b) one concludes that the spectral radius is zero when the reference damping matrix is taken as

$$[C_{\text{ref}}] = [C_\infty] + \frac{\beta \Delta t}{\gamma}([K_\infty] - [K_{\text{ref}}] + [S^0_{\text{r}}]\Delta t) + \frac{1}{\gamma \Delta t}([M_\infty] - [M_{\text{ref}}]) \tag{28}$$

It should be noted that the condition in equation (28) ensures that the pseudo-forces at step n are not a function of $\{u_b(n)\}$, which is sufficient for convergence, but does not imply that the pseudo-forces are zero. In particular, the magnitude of the pseudo-forces, and as a result, the number of iterations required to attain convergence, depend on the particular selection of $[K_{\text{ref}}]$ and $[M_{\text{ref}}]$. For efficiency, therefore, these matrices should be selected to approximate the real part of the impedance at the lower frequencies that dominate the response. The fact that the criteria in equation (28) is independent of the extent or distribution of inelastic behaviour is a feature that is worth noting explicitly.

It must be emphasized that the computation of the reference damping with equation (28) is not necessary for a successful implementation of the HTFD procedure. In particular, results from numerical simulations

have consistently indicated that convergence is attained without difficulty when $[K_{\text{ref}}] = [K_{\text{stat}}]$, $[M_{\text{ref}}] = [0]$ and $[C_{\text{ref}}] = [C_\infty]$, where $[K_{\text{stat}}]$ is the static stiffness. The previous selection is, of course, readily recognized as the doubly asymptotic approximation often used to model the unbounded domain with frequency independent parameters.

4. VALIDATION OF THE CONVERGENCE ANALYSIS

To test the equations developed in the stability analysis it is necessary to ensure that the computation of $\{R_b\}$ provides results that are in close agreement with those from equation (13). Although the use of equations (6) and (7) together with the implementation issues discussed in Section 2.1 provides sufficient accuracy in actual applications, to test the convergence of the HTFD procedure at values of ρ near unity the procedure must be complemented with a strategy that controls the magnitude of the displacements during iterations. The need for this control can be appreciated by noting that the HTFD method converges in a time progressive manner (i.e. convergence is attained at time t only after the response has converged at previous times) and that, if $\{u_b\}$ becomes sufficiently large ahead of the converged front, it eventually disrupts the converged part of the solution. The tests of stability presented next, for ρ values near unity, are carried out using a segmentation strategy analogous to that routinely used in applications of the hybrid-frequency-time domain procedure.[9]

4.1. Validation of equation (28)

The structure selected for the numerical simulation is an eight-storey uniform shear building founded on a rigid mat at the surface of a soil layer fixed at its base. A stringent test is realized by selecting $[K_{\text{ref}}] = [M_{\text{ref}}] = [0]$, which represents a statically unstable system. The free field excitation is taken as the acceleration pulse shown in Figure 4. The iterations are carried out over the complete duration of the analysis which is taken as 1·6 s. The parameter χ, defined as the largest absolute value of the difference in the displacement history from successive iterations, normalized by the maximum value in the current iteration (maximum over all DOF) is used to display the evolution of the solution as the number of iterations increases. The results are presented in Figure 6 for two cases, elastic behavior and a case where the yield level of the first three storeys equals 1/4 of the maximum associated elastic shears. The integrations are carried out using the CAA method ($\gamma = 1/2$, $\beta = 1/4$) using a time step of 0·02 s.

As the results depicted in Figure 6 show, the solution converges in both cases. It is worth noting that the initial increase in χ is simply a byproduct of its definition and of the fact that, as pointed out previously, the HTFD procedure converges in a time progressive manner.

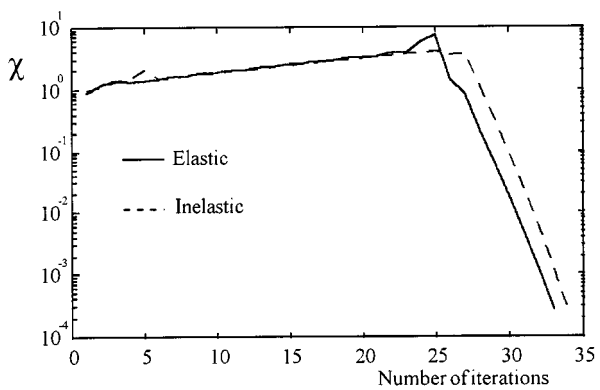

Figure 6. χ versus number of iterations (building of Figure 3 subjected to the pulse in Figure 4 $[M_{\text{ref}}] = [K_{\text{ref}}] = [0]$, $[C_{\text{ref}}]$ from equation (28)); inelastic case is associated with yielding in the lower three storeys)

4.2. Finite values of ρ

The stability criterion is tested in this section for finite ρ values. The spectral radius for the building in Figure 3 was initially computed using $[M_{\text{ref}}] = [0]$, $[K_{\text{ref}}] = [K_{\text{stat}}]$ and by taking $[C_{\text{ref}}]$ as the imaginary part of the impedance for a number of values of a_0 in the range $0 < a_0 < 4$. The results showed, however, that for these conditions $\rho \leqslant 1$ for all values of a_0 so convergence is expected always. Since the objective here is to further test the convergence criterion, ρ was forced upwards artificially by reducing the coefficients of the matrix $[M_{bb}]$ to 10 per cent of their actual values. A plot of ρ, as a function of the dimensionless frequency used to evaluate $[C_{\text{ref}}]$, is depicted in Figure 7 for the structure with the reduced $[M_{bb}]$. Results are shown for the soil layer and the halfspace and, in each case, for elastic behavior and for the case of yielding in the first three storeys. As can be seen, spectral radius larger than unity are attained for all the conditions when $[C_{\text{ref}}]$ is based on sufficiently small values of a_0.

Two observations from the results plotted in Figure 7 are appropriate. First, for low values of the dimensionless frequency, the value of ρ is much larger for the layer than for the halfspace. This behaviour is a result of the cutoff frequency displayed by the impedance of the layer. Second, although yielding leads to a notable increase in ρ when a_0 is small, the effect of inelasticity in the spectral radius is small in the range where the anticipated response is stable.

Results of simulations for $\rho = 0{\cdot}5$, $0{\cdot}9$ and $1{\cdot}1$ are summarized in Table I. As expected, the number of iterations to attain convergence is large when $\rho = 0{\cdot}9$ and segmentation of the time axis becomes necessary to prevent a disruption of the solution from the periodicity in equations (6) and (7). When $[C_{\text{ref}}]$ is selected such that $\rho = 0{\cdot}5$, however, convergence is attained with a few iterations without the need for segmentation. As expected, divergence occurs when $\rho > 1$.

5. EFFICIENCY OF THE HTFD PROCEDURE

In this section the efficiency of the HTFD approach is compared to that of the hybrid-frequency-time-domain technique in the context of a particular example. The structure is again taken as the eight-storey shear building of Figure 3. Results are computed for three different levels of inelastic behavior using the first 15 s of El Centro (1940) as the free field excitation. Some insight on how the degree of frequency dependency affects the number of iterations is obtained by considering the half-space and the layer with $d/r_0 = 2$. The matrices that define the reference impedance for the analyses with the HTFD are taken as $[K_{\text{ref}}] = [K_{\text{stat}}]$, $[C_{\text{ref}}]$ = damping at the Nyquist Frequency and $[M_{\text{ref}}] = [0]$.

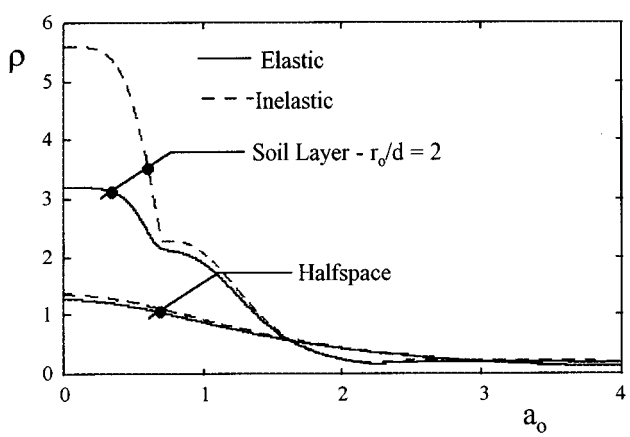

Figure 7. Spectral radius vs. dimensionless frequency used to compute the reference damping (building in Figure 3 with $[M_{bb}]$ taken as 10% of values listed; $\gamma = 1/2$, $\beta = 1/4$, $\Delta t = 0{\cdot}02$ s; inelastic case is associated with yielding in the lower three storeys)

Table I. Number of iterations to reach $\chi \leqslant 0{\cdot}001$ for the building in Figure 3 (excitation is the pulse in Figure 4; inelastic case involves yielding in the lower three stories, $\gamma = 1/2$, $\beta = 1/4$, $\Delta t = 0{\cdot}02$ s)

	Foundation			
	Half-space		Soil layer	
ρ	Elastic structure	Inelastic structure	Elastic structure	Inelastic structure
1·1	Divergence	Divergence	Divergence	Divergence
0·9	460	332	512	386
0·5	4	5	7	7

Table II. Comparison of efficiency between the HTFD procedure and the hybrid-frequency-time-domain approach (building-foundation system of Figure 3)

	HTFD				Hybrid-frequency-time-domain			
	Half-space		Soil layer		Half-space		Soil layer	
Q	No. of iterations	CPU (s)	No. of iterations	CPU (s)	No. of iterations	CPU (s)	No. of iterations	CPU (s)
1	4	135·2	7	217·9	1	25·4	1	25·4
2	4	136·7	7	219·4	103	797·5	105	826·3
4	4	142·3	6	212·5	225	1821·7	235	1920·9
6	4	138·7	6	194·0	340	2641·4	310	2463·2

The results are summarized in Table II. The value of Q in the first column is defined as the ratio of the maximum elastic storey shears to the yield shear. The same value is used in every storey. The trends that one anticipates from the nature of both techniques are evident in the results depicted. In particular, in the HTFD procedure the number of iterations required to attain convergence are larger for the soil layer than for the halfspace and are essentially independent of the degree of inelasticity in the response. In contrast, in the solutions with the hybrid-frequency-time-domain the number of iterations is insensitive to the nature of the impedance but increases with the extent of inelastic action. The CPU times associated with the solutions using the HTFD approach are, however, smaller than those demanded by the hybrid-frequency-time-domain procedure in all cases where the response is inelastic. In particular, for the conditions examined in this example, the HTFD procedure proves to be between 4 and 19 times faster than the hybrid-frequency-time domain approach. Although not shown, the solutions obtained with either technique are found virtually identical.

While the bulk of the advantage of the HTFD procedure over a hybrid solution in the frequency domain derives from the reduced number of iterations, it is worth noting that the required duration of the analysis can also play a role. Specifically, while the computations in the HTFD procedure are carried out for the time of desired results (15 s in the example shown), in the hybrid-frequency-time-domain method it is typically necessary to pad the loading with zeros to allow for the decay of free vibration. Since damping in the structure is typically small, the length of the required quiet zone is often significant. While special techniques to bring the periodic solution into coincidence with the transient without extending the duration of the analysis exist, their incidence on the relative efficiency between the HTFD procedure and the hybrid-frequency-time-domain approach was not explored in this pilot study.

6. CONCLUSIONS

1. The HTFD approach provides a particularly simple alternative for obtaining rigorous solutions for inelastic SSI problems. The method uses conventional time step algorithms to solve the equations of motion and adjusts for the frequency dependency of the soil medium using the pseudo-force approach. Implementation of the procedure into standard step-by-step non-linear analysis programs is straightforward.
2. In the HTFD procedure the pseudo-forces are restricted to the DOF at the soil–structure interface. An important by-product of this result is the fact that the analysis of convergence can be carried in a system whose size is limited to the number of DOF at this interface.
3. A convergence criterion for the HTFD method is derived. As is often the case, the criterion is expressed as a limit of unity on the spectral radius ρ of an appropriately defined matrix. It is shown that inelastic behavior enters into the evaluation of ρ as changes in the partition of the structural stiffness associated with the DOF at the base. Although reductions in the coefficients of this matrix due to yielding increase ρ, the effect is typically small.
4. It is found that the selection of the static stiffness and the damping at high frequency as the reference impedance typically results in small values of ρ for which convergence is attained without difficulty. An expression for a reference damping matrix that forces the spectral radius to zero and thus guarantees convergence is, however, presented. Although evaluation of this reference damping requires identification of the singular impedance, the matrix does not depend on the extent or distribution of inelasticity during the response.
5. Segmentation of the time axis, a technique typically needed for a successful implementation of the hybrid-frequency-time-domain procedure, was found unnecessary in the case of the HTFD approach.
6. Numerical results obtained for an eight-storey shear building show that the HTFD procedure can provide significantly more efficient solutions that the alternative hybrid-frequency-time-domain approach when the anticipated response is inelastic. In particular, the HTFD domain proved to be between 4 and 19 times faster than the hybrid-frequency-time-domain procedure in the simulations considered.

ACKNOWLEDGMENT

A significant portion of the research reported in this paper was carried out while the first author was on Sabbatical leave at the Polytechnic University in Madrid, Spain. The generous support provided by the Spanish Ministry of Education and Research during this period is gratefully acknowledged.

REFERENCES

1. J. P. Wolf, *Dynamic Soil–Structure Interaction*, Prentice-Hall, Englewood Cliffs, NJ, 1985.
2. B. Verbic, 'Analysis of certain structure–foundation interaction systems', *Ph.D. Thesis*, Rice University, Houston, TX, 1972.
3. J. P. Wolf and P. Obernhuber, 'Non-linear soil–structure analysis using dynamic stiffness of flexibility of soil in the time domain', *Earthquake Engng. Struct. Dyn.* **13**, 195–212 (1985).
4. J. P. Wolf, *Soil–Structure-Interaction Analysis in Time Domain*, Prentice-Hall, Englewood Cliffs, NJ, 1988.
5. S. K. Mohasseb and J. P. Wolf, 'Recursive evaluation of interaction forces of unbounded soil in frequency domain', *Soil Dyn. Earth. Engng.* **8**(4), 176–188 (1989).
6. J. P. Wolf and M. Motosaka, 'Recursive evaluation of interaction forces of unbounded soil in the time domain', *Earthquake Engng. Struct. Dyn.* **18**, 345–363 (1989).
7. J. P. Wolf and M. Motosaka, 'Recursive evaluation of interaction forces of unbounded soil in the time domain from dynamic coefficients in the frequency domain', *Earthquake Engng. Struct. Dyn.* **18**, 365–376 (1989).
8. J. D. Kawamoto, 'Solution of nonlinear dynamic structural system by a hybrid frequency-time-domain approach', *Research Report R 83-5*, Massachusetts Institute of Technology, Department of Civil Engineering, Cambridge, MA, 1983.
9. G. R. Darbre and J. P. Wolf, 'Criterion of stability and implementation issues of hybrid frequency-time domain procedure for nonlinear dynamic analysis', *Earthquake Engng. Struct. Dyn.* **16**, 569–581 (1988).
10. G. R. Darbre, 'Seismic analysis of non-linearly base-isolated soil–structure interacting reactor building by way of the hybrid-frequency-time-domain procedure', *Earthquake Engng. Struct. Dyn.* **19**, 725–738 (1990).

11. G. R. Darbre, 'Application of the hybrid frequency time domain procedure to the soil–structure interaction analysis of a shear building with multiple nonlinearities', *Proc. 5th Int. Conf. on Soil Dynamics and Earthquake Engineering*, Karlsruhe, 1991, pp. 441–454.
12. J. W. Chavez and G. L. Fenves, 'Earthquake analysis of concrete gravity dams including base sliding', *Earthquake Engng. Struct. Dyn.* **24**, 673–686 (1995).
13. G. L. Fenves and J. W. Chavez, 'Hybrid-frequency-time-domain analysis of nonlinear fluid–structure systems', *Proc 4th U.S. National Conf. on Earthquake Engineering*, 1990.
14. J. P. Wolf, 'Spring-dashpot-mass models for foundation vibrations', *Earthquake Engng. Struct. Dyn.* **26**, 931–949 (1997).
15. A. S. Veletsos and B. Verbic, 'Basic response functions for elastic foundations', *J. Engng. Mech. ASCE*, **100**(EM2), 189–201 (1974).
16. A. Papoulis, *The Fourier Integral and its Applications*, McGraw-Hill, New York, 1987.

